On the spectral efficiency of a sphere

Gustafsson, Mats; Nordebo, Sven

2004

CODEN:LUTEDX/(TEAT-7127)/1-24/(2004)

On the spectral efficiency of a sphere

Mats Gustafsson and Sven Nordebo

Department of Electroscience
Electromagnetic Theory
Lund Institute of Technology
Sweden

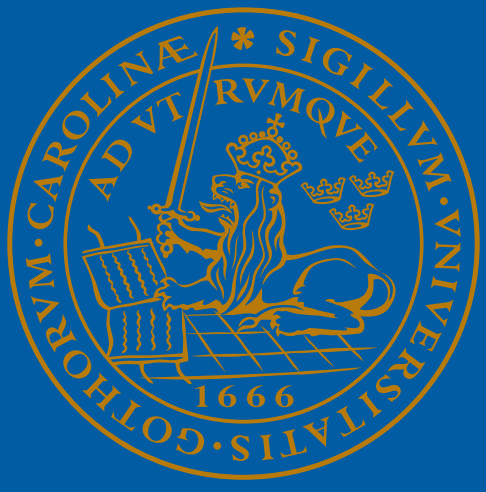

Mats Gustafsson

Department of Electroscience
Electromagnetic Theory
Lund Institute of Technology
P.O. Box 118
SE-221 00 Lund
Sweden

Sven Nordebo

School of Mathematics and System Engineering
Växjö University
Växjö
Sweden

Editor: Gerhard Kristensson

Abstract

In many cases it is desired to have both high capacity and small antennas in wireless communication systems. Unfortunately, the antenna performance deteriorate when the antennas get electrically small. In this paper fundamental limitations from antenna theory and broadband matching are used to analyze the spectral efficiency of an arbitrary antenna inserted inside a sphere.

1 Introduction

The spectral efficiency of a wireless communication system is determined by the properties of the channel that relates the transmitted and received signals. This communication channel is in general very complicated and depends on the feeding network, the antennas, and the wave propagation between the antennas. Recently, the multiple-input multiple-output (MIMO) systems have received much interest due to their ability to increase the spectral efficiency in wireless communication systems [8, 21, 27]. The MIMO systems are based on the use of multiple antennas at each end of the communication link in environments with rich multi-path propagation.

In many cases it is desired to design systems that both have a high capacity and a small physical size. Unfortunately, the antenna performance deteriorates when the antenna gets electrically small [13, 27]. Fundamental limitations on this kind of systems can be analyzed under various assumptions. The case with idealized antennas, *i.e.*, antennas that do not interact with the electromagnetic field, are, *e.g.*, discussed in [17, 19, 28]. In the planar case, a plane wave expansion shows that the idealized antennas are correlated at distances less than half the wavelength λ, giving a preferred antenna-array element spacing of approximately $\lambda/2$. Although, also the volume case [19] can be analyzed with idealized antennas, it is preferable to consider a model that includes the properties of the antennas. In this paper, fundamental limitations on the capacity of an arbitrary antenna inserted inside a sphere are analyzed.

To analyze the spectral efficiency of a volume, it is essential to relate three classical theories giving fundamental limitations in the disciplines information theory, broadband matching, and antenna theory. In information theory, the Shannon theory set fundamental limits of how coding can be used to increase the data rate over a given communication channel, *i.e.*, the capacity [24]. The capacity depends on the number and gain of the orthogonal sub channels and their signal to noise ratio [21]. For the spectral efficiency of a volume, the interesting channel is the channel that relates the signals on transmission lines to the electromagnetic wave field outside the volume. Of course, this channel depends on the choice of antennas, matching, transmission lines, and the statistics of the radio channel outside the volume. Here, it is essential to consider the best possible antenna in the given volume as well as the best possible matching to a transmission line. The classical theory of broadband matching, shows how much power that can be transmitted between a transmission

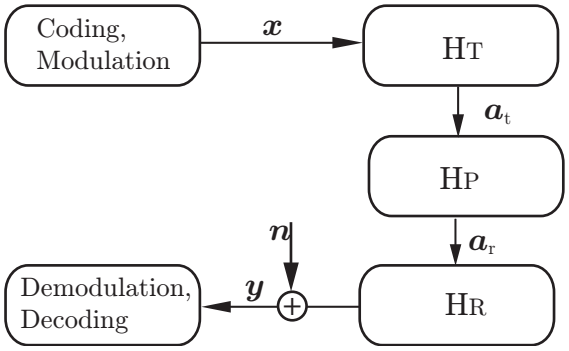

Figure 1: Block scheme of a wireless communication system. The output is $\boldsymbol{y} = \mathbf{H}\boldsymbol{x} + \boldsymbol{n}$, where the channel is decomposed into the parts $\mathbf{H} = \mathbf{H}_{\mathrm{R}}\mathbf{H}_{\mathrm{P}}\mathbf{H}_{\mathrm{T}}$ and $\boldsymbol{n}$ is the noise.

line and a given load [9], *i.e.*, the antenna. The classical theory of radiation-Q uses spherical vector modes to analyze the properties of a hypothetical antenna inside a sphere [5, 13, 14]. An antenna with a high Q-factor has electromagnetic fields with large amounts of stored energy around it, and, hence, typically low bandwidth and high losses [13]. The mode expansion also gives a natural expression of the polarization, angle, and spatial diversity that is utilized in MIMO systems [8, 21, 25, 27].

In this paper the spectral efficiency of a sphere is analyzed. In Section 2, a decomposition of the communication channel into a transmitting antenna channel, a wave propagation channel, and a receiving antenna channel is given. The antenna channels relate the electrical signals on transmission lines to the electromagnetic fields outside the antennas. The electromagnetic field is represented by spherical vector waves. In Section 3, it is shown that a set of unpolarized uniformly distributed plane waves impinging on the antennas can be represented by a Rayleigh channel in the spherical vector modes. In Section 4, the Fano theory is used to get fundamental limitations on the matching network for low order spherical vector modes and resonance circuits. The capacity of a Rayleigh fading antenna channel is analyzed in Section 5. In Section 5.1, the MIMO cube and MIMO tetrahedron are analyzed with the spherical vector modes.

2 Channel decomposition and spherical vector mode representation

A MIMO–model for a communication system with N_{x} transmitting antennas and N_{y} receiving antennas is considered, as depicted in Figure 1. Here, $\boldsymbol{x}$ is the transmitted $N_{\mathrm{x}} \times 1$ signal, and $\boldsymbol{y}$ is the received $N_{\mathrm{y}} \times 1$ signal given by

$$\boldsymbol{y} = \mathbf{H}\boldsymbol{x} + \boldsymbol{n}, \tag{2.1}$$

where $\mathbf{H}$ is the complex $N_{\mathrm{y}} \times N_{\mathrm{x}}$ matrix, and $\boldsymbol{n}$ is complex Gaussian noise [20, 21, 27] with covariance matrix $\sigma_v^2\mathbf{I}$. The totally transmitted power is $P = \mathrm{trace}\{\mathbf{R}_{xx}\}$ where $\mathbf{R}_{xx}$ is the covariance matrix for the input signal $\boldsymbol{x}$.

To separate the antenna properties from the properties of the wave propagation, the communication channel is decomposed into a combination of a transmitting antenna channel $\mathbf{H}_{\mathrm{T}}$, a wave propagation channel $\mathbf{H}_{\mathrm{P}}$, and a receiving antenna channel $\mathbf{H}_{\mathrm{R}}$, *i.e.*, $\mathbf{H} = \mathbf{H}_{\mathrm{R}}\mathbf{H}_{\mathrm{P}}\mathbf{H}_{\mathrm{T}}$.

In particular, we can make the following assumptions. The communication distance is large enough so that there is no mutual coupling between the transmitting and receiving antenna arrays. The transmitted electric field $\boldsymbol{E}^{(\mathrm{t})}(\boldsymbol{r})$ can therefore be expanded in *outgoing spherical vector waves* $\boldsymbol{u}_{\tau ml}(k\boldsymbol{r})$

$$\begin{aligned}\boldsymbol{E}^{(\mathrm{t})}(\boldsymbol{r}) &= k\sqrt{2\eta}\sum_{l=1}^{\infty}\sum_{m=-l}^{l}\sum_{\tau=1}^{2} a_{\tau ml}^{(\mathrm{t})}\boldsymbol{u}_{\tau ml}\big(k(\boldsymbol{r}-\boldsymbol{r}_{\mathrm{t}})\big) \\ &= k\sqrt{2\eta}\sum_{\alpha} a_{\alpha}^{(\mathrm{t})}\boldsymbol{u}_{\alpha}\big(k(\boldsymbol{r}-\boldsymbol{r}_{\mathrm{t}})\big), \text{ for } |\boldsymbol{r}-\boldsymbol{r}_{\mathrm{t}}| \geq R_{\mathrm{t}} \quad (2.2)\end{aligned}$$

where the propagation region is assumed to be source–free, $a_{\tau ml}^{(\mathrm{t})} = a_{\alpha}^{(\mathrm{t})}$ are the expansion coefficients, $\boldsymbol{r}_{\mathrm{t}}$ is the position of the transmitting antenna array, R_{t} the radius of a sphere containing the antenna, k the wave number, and η the free space impedance. To simplify the notation, the multi–index $\alpha = (\tau, m, l)$ is used. Whenever necessary, the multi–index α is ordered and identified with the number $\alpha = 2(l^2+l-1+m)+\tau$, see also (5.7). The multi–poles are classified as either TE ($\tau = 1$) or TM ($\tau = 2$). The azimuthal and radial dependencies are given by the m and l index, respectively. The normalization with $k\sqrt{2\eta}$ is used to give a power normalization of the expansion coefficients, *i.e.*, the totally radiated power is given by $\sum_{\alpha}|a_{\alpha}|^2$.

We assume that the transmitting antenna channel is given by a linear mapping from the input signal $\boldsymbol{x}$ to the expansion coefficients $a_{\alpha}^{(\mathrm{t})}$, and can therefore be represented as

$$\boldsymbol{a}^{(\mathrm{t})} = \mathbf{H}_{\mathrm{T}}\boldsymbol{x}, \quad (2.3)$$

where we employ a semi–infinite notation for the column vector $\boldsymbol{a}^{(\mathrm{t})} = [a_{\alpha}^{(\mathrm{t})}]$ and the matrix $\mathbf{H}_{\mathrm{T}}$ which has N_{x} columns.

We assume that the received electric field $\boldsymbol{E}^{(\mathrm{r})}(\boldsymbol{r})$ can be expanded in *incoming spherical vector waves* $\boldsymbol{v}_{\alpha}(k\boldsymbol{r})$

$$\boldsymbol{E}^{(\mathrm{r})}(\boldsymbol{r}) = \sqrt{2\eta}\,k\sum_{\alpha} a_{\alpha}^{(\mathrm{r})}\boldsymbol{v}_{\alpha}\big(k(\boldsymbol{r}-\boldsymbol{r}_{\mathrm{r}})\big), \text{ for } |\boldsymbol{r}-\boldsymbol{r}_{\mathrm{r}}| \geq R_{\mathrm{r}}, \quad (2.4)$$

where $a_{\alpha}^{(\mathrm{r})}$ are the expansion coefficients, the multi–index $\alpha = (\tau, m, l)$ is employed as in (2.2), $\boldsymbol{r}_{\mathrm{r}}$ is the position of the receiving antenna array and R_{r} the radius of a sphere containing the antenna. The incoming spherical vector waves $\boldsymbol{v}_{\alpha}(k\boldsymbol{r})$ have the same basic features as the outgoing $\boldsymbol{u}_{\alpha}(k\boldsymbol{r})$ mentioned above.

The wave propagation channel $\mathbf{H}_{\mathrm{P}}$ contains the properties of the geometrical and electrical features between the transmitting antenna and the receiving antenna. In particular, the channel $\mathbf{H}_{\mathrm{P}}$ represents the mapping from the transmitted electric field $\boldsymbol{E}^{(\mathrm{t})}(\boldsymbol{r})$ to the received electric field $\mathbf{E}^{(\mathrm{r})}(\boldsymbol{r})$, or equivalently, the mapping from

the expansion coefficients $a_\alpha^{(\mathrm{t})}$ to $a_\alpha^{(\mathrm{r})}$. We assume that this mapping is linear, and can therefore be represented as

$$\boldsymbol{a}^{(\mathrm{r})} = \mathbf{H}_{\mathrm{P}} \boldsymbol{a}^{(\mathrm{t})}, \tag{2.5}$$

where the matrix $\mathbf{H}_{\mathrm{P}}$ is (countably) infinite–dimensional in both rows and columns. In practice however, and as we will see later, this matrix can be considered finite and represents as many modes that are practically relevant. The bandwidth of higher order modes will ultimately tend to zero as the corresponding Q–factors tend to infinity, and these modes will therefore not contribute to the capacity of the communication channel.

We assume that the receiving antenna channel is given by a linear mapping from the expansion coefficients $a_\alpha^{(\mathrm{r})}$ to the received signal $\boldsymbol{y}$, and can hence be represented as

$$\boldsymbol{y} = \mathbf{H}_{\mathrm{R}} \boldsymbol{a}^{(\mathrm{r})}, \tag{2.6}$$

where the semi–infinite matrix $\mathbf{H}_{\mathrm{R}}$ has N_{y} rows. Finally, the received signal $\boldsymbol{y}$ is corrupted by white Gaussian noise (2.1).

3 The Rayleigh fading antenna channel

The Rayleigh channel is most naturally defined as a channel with uncorrelated and zero mean entries having complex Gaussian distribution and the amplitudes thus being Rayleigh distributed [20–22, 27], *i.e.*, $\mathbf{H} = \mathbf{H}_{\mathrm{w}}$, where $\mathcal{E}\{\mathbf{H}_{\mathrm{w}}\} = 0$ and $\mathcal{E}\{\mathbf{H}_{\mathrm{w}}|_{ij} \mathbf{H}_{\mathrm{w}}^*|_{mn}\} = \delta_{im}\delta_{jn}$. However, it is also customary to derive this property from the assumption that a large number of independent and uniformly distributed scattered waves are incident on the receiver, see *e.g.*, [16]. Here, it is shown that a set of unpolarized uniformly distributed plane waves impinging on the antennas can be represented by a Rayleigh channel in the spherical modes.

Consider the channel from the transmitted signals to the received spherical vector modes, *i.e.*, $\mathbf{H}_{\mathrm{P}}\mathbf{H}_{\mathrm{T}}$. Suppose that the received electric field (2.4) is given by

$$\boldsymbol{E}^{(\mathrm{r})}(\boldsymbol{r}) = \sum_{n=1}^{N_{\mathrm{s}}} s_n \boldsymbol{E}_n \mathrm{e}^{-\mathrm{i}k\hat{\boldsymbol{k}}_n \cdot (\boldsymbol{r} - \boldsymbol{r}_{\mathrm{r}})}, \text{ for } |\boldsymbol{r} - \boldsymbol{r}_{\mathrm{r}}| \geq R_{\mathrm{r}} \tag{3.1}$$

consisting of a number of uniformly distributed and independent scattered plane wave components. Here s_n represents the complex signal amplitudes, $\boldsymbol{E}_n$ random field strengths, and the time convention $\mathrm{e}^{\mathrm{i}\omega t}$ is used.

It is assumed that for each fixed direction $\hat{\boldsymbol{k}}_n$, the field $\boldsymbol{E}_n$ has zero-mean complex Gaussian components with the variance E_0^2, *i.e.*, $\boldsymbol{E}_n = E_0(\phi_1 \hat{\boldsymbol{u}}_1 + \phi_2 \hat{\boldsymbol{u}}_2)$, where $\hat{\boldsymbol{u}}_1$ and $\hat{\boldsymbol{u}}_2$ are two orthogonal unit vectors that are perpendicular to $\hat{\boldsymbol{k}}_n$ and ϕ_i have variance 1. This means that the polarization of $\boldsymbol{E}_n$ is uniformly distributed over the Poincare sphere, *i.e.*, *unpolarized*, with the *Stokes parameter* $E_0^2 = \mathcal{E}\{|\boldsymbol{E}_n|^2\}$. The average power flux is given by $E_0^2/(2\eta)$. It is furthermore assumed that the incident directions $\hat{\boldsymbol{k}}_n$ are uniformly distributed over the unit sphere.

The wave propagation channel $\mathbf{H}_{\mathrm{P}}$ can be decomposed into two parts $\mathbf{H}_{\mathrm{P}} = \mathbf{H}_{\mathrm{A}}\mathbf{H}_{\mathrm{B}}$ where $\mathbf{H}_{\mathrm{B}}$ represents the mapping from $a_\alpha^{(\mathrm{t})}$ to s_n coefficients, and $\mathbf{H}_{\mathrm{A}}$ represents the mapping from s_n coefficients to $a_\alpha^{(\mathrm{r})}$. Thus,

$$\boldsymbol{a}^{(\mathrm{r})} = \mathbf{H}_{\mathrm{A}}\boldsymbol{s} \tag{3.2}$$

where the mapping (3.2) is defined by the expansion of plane waves in incoming spherical vector waves

$$a_\alpha^{(\mathrm{r})} = \frac{1}{\sqrt{2\eta}\,k}\sum_{n=1}^{N_{\mathrm{A}}} 2\pi \mathrm{i}^{1-\tau-l}\boldsymbol{A}_\alpha^*(\hat{\boldsymbol{k}}_n)\cdot\boldsymbol{E}_n s_n \tag{3.3}$$

and we can conclude that

$$\mathbf{H}_{\mathrm{A}}|_{\alpha n} = \frac{2\pi}{\sqrt{2\eta}\,k}\mathrm{i}^{1-\tau-l}\boldsymbol{A}_\alpha^*(\hat{\boldsymbol{k}}_n)\cdot\boldsymbol{E}_n. \tag{3.4}$$

The channel $\mathbf{H}_{\mathrm{A}}$ is a random channel. With the assumption above of uniformly distributed unpolarized waves, the expectation of each channel element is zero, *i.e.*, $\mathcal{E}\left\{\mathbf{H}_{\mathrm{A}}|_{\alpha n}\right\} = 0$. The expectation of the channel product elements $\mathbf{H}_{\mathrm{A}}|_{\alpha n}\mathbf{H}_{\mathrm{A}}^*|_{\alpha' n'}$ can be written

$$\begin{aligned}\mathcal{E}\left\{\mathbf{H}_{\mathrm{A}}|_{\alpha n}\mathbf{H}_{\mathrm{A}}^*|_{\alpha' n'}\right\} &= \frac{2\pi^2}{\eta k^2}\mathrm{i}^{l'-l+\tau'-\tau}\mathcal{E}\left\{\boldsymbol{A}_\alpha^*(\hat{\boldsymbol{k}}_n)\cdot\boldsymbol{E}_n\boldsymbol{A}_{\alpha'}(\hat{\boldsymbol{k}}_{n'})\cdot\boldsymbol{E}_{n'}^*\right\}\\ &= \frac{2\pi^2}{\eta k^2}\mathrm{i}^{l'-l+\tau'-\tau}\mathcal{E}_{\hat{\boldsymbol{k}}}\left\{\boldsymbol{A}_\alpha^*(\hat{\boldsymbol{k}}_n)\cdot\mathcal{E}_{\boldsymbol{E}}\left\{\boldsymbol{E}_n\boldsymbol{E}_{n'}^*\right\}\cdot\boldsymbol{A}_{\alpha'}(\hat{\boldsymbol{k}}_{n'})\right\}. \end{aligned}\tag{3.5}$$

The expectation over the polarization is

$$\mathcal{E}_{\widetilde{\boldsymbol{E}}}\left\{\boldsymbol{E}_n^*\widetilde{\boldsymbol{E}}_{n'}\right\} = \mathcal{E}\left\{|\boldsymbol{E}_n|^2\right\}\mathbf{I}_{2\times 2}\delta_{nn'} = E_0^2\mathbf{I}_{2\times 2}\delta_{nn'}, \tag{3.6}$$

where $\mathbf{I}_{2\times 2}$ denotes the 2 by 2 identity dyad. The expectation over the incident angles is hence

$$\begin{aligned}\mathcal{E}\left\{\mathbf{H}_{\mathrm{A}}|_{\alpha n}\mathbf{H}_{\mathrm{A}}^*|_{\alpha' n'}\right\} &= \frac{2\pi^2 E_0^2}{\eta k^2}\mathrm{i}^{l'-l+\tau'-\tau}\mathcal{E}_{\hat{\boldsymbol{k}}}\left\{\boldsymbol{A}_\alpha^*(\hat{\boldsymbol{k}}_n)\cdot\boldsymbol{A}_{\alpha'}(\hat{\boldsymbol{k}}_n)\right\}\delta_{nn'}\\ &= \frac{\pi E_0^2}{2\eta k^2}\mathrm{i}^{l'-l+\tau'-\tau}\delta_{nn'}\int_\Omega \boldsymbol{A}_\alpha^*(\hat{\boldsymbol{r}})\cdot\boldsymbol{A}_{\alpha'}(\hat{\boldsymbol{r}})\,\mathrm{d}\Omega = \frac{\pi E_0^2}{2\eta k^2}\delta_{\alpha\alpha'}\delta_{nn'}\end{aligned}\tag{3.7}$$

Here, it is essential to normalize the SNR to the total power of the electromagnetic wave that impinges on the sphere. Although the power of a plane wave is infinite any finite mode expansion represents a finite amount of power. It is also necessary to consider the distribution of the average amplitude as a function of frequency. Here, we assume that the amplitude decay is proportional to the propagation distance in wavelengths, *i.e.*, E_0/k is constant. This can be interpreted as a power normalization with respect to the The plane wave is normalized with respect to the power flux

through the cross section of the sphere with radius $\lambda/(2\pi) = k^{-1}$. To simplify the notation, the average power per plane wave is defined as

$$\frac{P}{N_{\rm s}} = \frac{E_0^2 \pi}{2\eta k^2} \tag{3.8}$$

In conclusion, the fundamental Rayleigh channel $\mathbf{H}_{\rm A}$ defined in (3.1) though (3.3) has complex Gaussian entries, *i.e.*, $\mathbf{H}_{\rm A} = \sqrt{\frac{P}{N_{\rm s}}}\mathbf{H}_{\rm w}$. The trace of the covariance matrix for the signal $\boldsymbol{s}$ is normalized as trace$\{\mathbf{R}_{ss}\} = N_{\rm s}$.

The received signal is hence given by

$$\begin{aligned}\boldsymbol{y} = \sqrt{\frac{P}{N_{\rm s}}}\mathbf{H}_{\rm R}\mathbf{H}_{\rm w}\boldsymbol{s} + \boldsymbol{n} = \sqrt{\frac{P}{N_{\rm s}}}\mathbf{H}_{\rm R}\mathbf{H}_{\rm w}\mathbf{H}_{\rm B}\mathbf{H}_{\rm T}\boldsymbol{x} + \boldsymbol{n} \\ = \sqrt{\frac{P}{N_{\rm s}}}\mathbf{H}_{\rm R}\mathbf{H}_{\rm w}\mathbf{R}_{\rm T}^{1/2}\boldsymbol{x} + \boldsymbol{n},\end{aligned} \tag{3.9}$$

where $\mathbf{R}_{\rm T}^{1/2}$ is the correlation matrix [21] on the transmitter side. It is also observed that $\mathbf{H}_{\rm R}$ can be interpreted as the square of the correlation matrix on the receiver side, *i.e.*, $\mathbf{H}_{\rm R} = \mathbf{R}_{\rm R}^{1/2}$.

Naturally the received power is much smaller than transmitted power in wireless communication systems. In the analysis of the receiving channel $\mathbf{H}_{\rm R}$ the channel model from random plane waves $\boldsymbol{s}$ to $\boldsymbol{y}$ in (3.9) is used. This is equivalent to the assumption of an uncorrelated channel on the transmitter side $\mathbf{R}_{\rm T} = \mathbf{I}$, see also Theorem B.1. This gives the channel

$$\boldsymbol{y} = \sqrt{\frac{P}{N_{\rm s}}}\mathbf{H}_{\rm R}\mathbf{H}_{\rm w}\boldsymbol{s} + \boldsymbol{n}. \tag{3.10}$$

It is noted that this channel model is independent of frequency as well as of the size of the receiving sphere.

A SVD of the receiving channel, $\mathbf{H}_{\rm R} = \mathbf{U}\boldsymbol{\Sigma}'\mathbf{V}^{\rm H}$, gives

$$\tilde{\boldsymbol{y}} = \mathbf{U}^{\rm H}\boldsymbol{y} = \sqrt{\frac{P}{N_{\rm s}}}\boldsymbol{\Sigma}'\mathbf{V}^{\rm H}\mathbf{H}_{\rm w}\boldsymbol{s} + \mathbf{U}^{\rm H}\boldsymbol{n}. \tag{3.11}$$

To simplify this channel model, we first observe that $\mathbf{V}^{\rm H}\mathbf{H}_{\rm w}$ is a semi-infinite Rayleigh matrix with $N_{\rm s}$ columns. Secondly, we let $\boldsymbol{\Sigma}$ denote the $N_{\rm y} \times N_{\rm y}$ diagonal matrix containing the singular values of the semi-infinite matrix $\boldsymbol{\Sigma}'$. Finally, the infinite matrix product in $\boldsymbol{\Sigma}'\mathbf{V}^{\rm H}\mathbf{H}_{\rm w}$ is replaced by a finite matrix product between $\boldsymbol{\Sigma}$ and a finite Rayleigh matrix. This gives the equivalent channel

$$\tilde{\boldsymbol{y}} = \sqrt{\frac{P}{N_{\rm s}}}\boldsymbol{\Sigma}\mathbf{H}_{\rm w}\boldsymbol{s} + \tilde{\boldsymbol{n}}, \tag{3.12}$$

where $\boldsymbol{\Sigma}$ and $\mathbf{H}_{\rm w}$ are an $N_{\rm y} \times N_{\rm y}$ diagonal matrix containing the singular values of $\mathbf{H}_{\rm R}$ and an $N_{\rm y} \times N_{\rm s}$ Rayleigh matrix, respectively.

Since the channel is random the corresponding information rate is a random variable. The capacity of these fading channels are commonly analyzed with the ergodic capacity and the outage capacity [21]. In this section, we do not consider the bandwidth of the system and hence use the capacity (efficiency) with the unit b/s/Hz as commonly used in MIMO literature. To avoid confusion with the capacity in b/s, we either give the units or use the word capacity efficiency whenever necessary.

The ergodic capacity (in b/s/Hz) of the channel (3.12) is given by

$$\overline{C} = \mathcal{E}\left\{\max_{\mathbf{R}_{ss}} \log_2 \det\left(\mathbf{I} + \frac{P}{N_0 N_\mathrm{s}} \mathbf{\Sigma}\mathbf{H}_\mathrm{w}\mathbf{R}_{ss}\mathbf{H}_\mathrm{w}^\mathrm{H}\mathbf{\Sigma}\right)\right\} \tag{3.13}$$

where $\mathbf{\Sigma}$ and $\mathbf{H}_\mathrm{w}$ are the diagonal matrix containing the singular values of $\mathbf{H}_\mathrm{R}$ and an $N_\mathrm{y} \times N_\mathrm{s}$ Rayleigh channel, respectively. The correlation matrix $\mathbf{R}_{ss}$ is given by the water-filling solution [21].

The case of an idealized antenna connecting each spherical vector mode to one port gives N_y uncorrelated sub-channels $\mathbf{\Sigma} = \mathbf{I}_{N_\mathrm{y} \times N_\mathrm{y}}$. The ergodic capacity, in b/s, is given by the ergodic capacity of the $\mathbf{H}_\mathrm{w}$ channel, *i.e.*,

$$\overline{C} = \mathcal{E}\left\{\max_{\mathbf{R}_{ss}} \log_2 \det\left(\mathbf{I} + \frac{P}{N_0 N_\mathrm{s}} \mathbf{H}_\mathrm{w}\mathbf{R}_{ss}\mathbf{H}_\mathrm{w}^\mathrm{H}\right)\right\} \tag{3.14}$$

The properties of this $\mathbf{H}_\mathrm{w}$ MIMO channel is analyzed in many papers, see *e.g.*, [21, 27]. A lower bound on the ergodic capacity is given by

$$\overline{C} \geq R \log_2\left(1 + \frac{P}{N_0 N_\mathrm{s}} \exp\left(\frac{1}{R}\sum_{j=1}^{R}\sum_{p=1}^{R'}\frac{1}{p} - \gamma\right)\right) \tag{3.15}$$

where $R = \min(N_\mathrm{y}, N_\mathrm{s})$, $R' = \max(N_\mathrm{y}, N_\mathrm{s})$, and $\gamma = 0.577...$ the Euler's constant [21]. Here, it it seen that the capacity efficiency of an antenna that connects each spherical vector mode to one port increases rapidly with the number of ports as long as the SNR is sufficiently high. It is also observed that the capacity efficiency is independent of the radius of the antenna. Since the number of spherical modes is infinite the number of spatial channels is also infinite irrespectively of the size of the volume. Obviously, this is unrealistic. To circumvent this problem the capacity has to be considered, *i.e.*, the capacity in b/s. The interpretation of the capacity (3.13) can be simplified by assuming an SNR, sufficiently high so that the identity matrix in (3.13) can be neglected. This gives

$$\overline{C} \approx \mathcal{E}\left\{\log_2 \det\left(\frac{P}{N_0 N_\mathrm{s}} \mathbf{H}_\mathrm{w}\mathbf{R}_{ss}\mathbf{H}_\mathrm{w}^\mathrm{H}\right)\right\} + \log_2 \det\left(\mathbf{\Sigma}^2\right). \tag{3.16}$$

The second term can be interpreted as the loss in ergodic capacity due to the antenna channel at a high SNR. The correlation loss is given by

$$\Delta\overline{C} = \log_2 \det\left(\mathbf{\Sigma}_\mathrm{R}^2\right) = \log_2 \prod_{m=1}^{N_\mathrm{y}} \sigma_m^2 = \sum_{m=1}^{N_\mathrm{y}} \log_2 \sigma_m^2 \tag{3.17}$$

Since the receiving antenna channel has a total power gain $\|\mathbf{\Sigma}\|_\mathrm{F}^2 \leq N_\mathrm{y}$ the correlation $\det \mathbf{\Sigma} \leq 1$ and hence $\Delta\overline{C} \leq 0$.

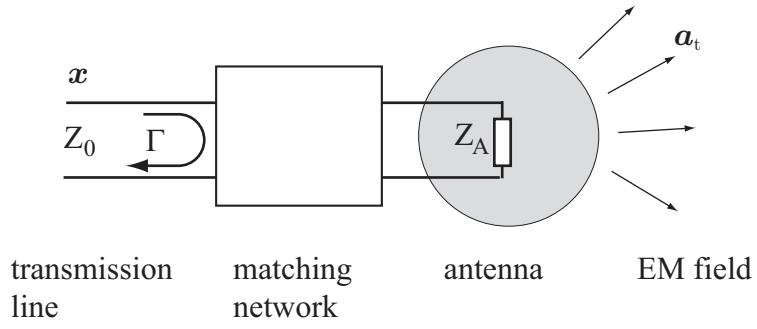

Figure 2: The transmitting (and receiving) antenna channel $\mathbf{H}_{\mathrm{T}}$ is the map from the electrical signals $\boldsymbol{x}$ on the transmission line to the radiated electromagnetic field outside the antenna, here represented by the spherical vector modes $\boldsymbol{a}_{\mathrm{t}}$.

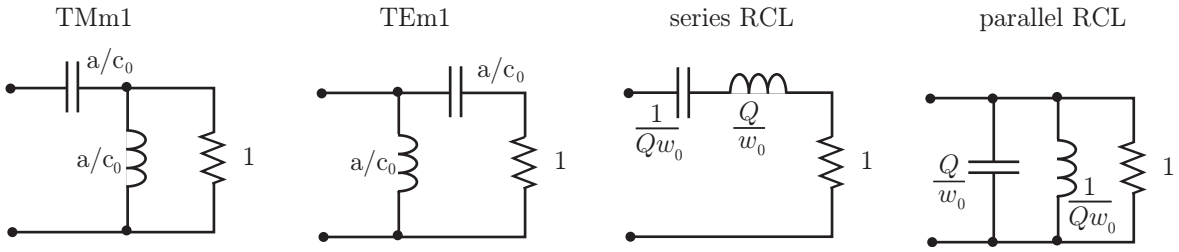

Figure 3: Circuit models of simple antennas. The resistor models the radiation part. The capacitor and inductor model the parts that stores the electric field and magnetic field, respectively. The inductance and capacitance of the lowest order modes are given by a/c_0, where a and c_0 are the sphere radius and speed of light, respectively.

4 Limitations on the antenna channel

The antenna channels connect the electrical signals on the transmission line with the radiated electromagnetic waves outside the antenna. This channel is in general very complex. Here, the case where each transmission line is connected to a spherical wave with a lossless matching network is considered, see Figure 2. From the input signal, the antenna can be modeled with a lumped circuit model. The spherical vector modes have a circuit equivalent representing the impedance of the modes [5, 14]. The equivalent circuits of the lowest order modes, *i.e.*, the TM_{m1} and TE_{m1} for $m = -1, 0, 1$, are shown in Figure 3. The resistance R, capacitance C, and inductance L are the circuit equivalents of the radiated field, the stored electric field, and the stored magnetic field, respectively. The higher order modes are given by a ladder network [5, 14]. These circuits can be interpreted as high-pass filters. The Fano theory is used to get fundamental limitations on the matching network [9, 26].

The Fano theory uses Taylor expansions of the reflection coefficient around the zeros of the transmission coefficient to get a set of integral relations for the reflection coefficient. Here, we assume that transmission line has unit impedance. The transmission coefficient of the TM_{m1} and TE_{m1} modes has a double zero at $s = 0$.

The corresponding reflection coefficient is

$$\Gamma_1(s) = \frac{1}{1 + \frac{2sa}{c_0} + \frac{2s^2a^2}{c_0^2}} \tag{4.1}$$

without zeros $\lambda_{\mathrm{o}i}$ but with the two poles

$$\lambda_{\mathrm{p}1,2} = \frac{-1 \pm \mathrm{i}}{\frac{2a}{c_0}} = \left(\frac{a}{c_0}(-1 \mp \mathrm{i})\right)^{-1}. \tag{4.2}$$

The coefficients of the Taylor series around $s = 0$ give the two integral relations

$$\frac{2}{\pi}\int_0^\infty \omega^{-2} \ln \frac{1}{|\Gamma(\mathrm{i}\omega)|}\,\mathrm{d}\omega = \sum_i \lambda_{\mathrm{o}i}^{-1} - \lambda_{\mathrm{p}i}^{-1} - 2\lambda_{\mathrm{r}i}^{-1} = \left(\frac{2a}{c_0} - 2\sum_i \lambda_{\mathrm{r}i}^{-1}\right) \tag{4.3}$$

and

$$\frac{2}{\pi}\int_0^\infty \omega^{-4} \ln \frac{1}{|\Gamma(\mathrm{i}\omega)|}\,\mathrm{d}\omega = -\frac{1}{3}\sum_i \lambda_{\mathrm{o}i}^{-3} - \lambda_{\mathrm{p}i}^{-3} - 2\lambda_{\mathrm{r}i}^{-3} = \left(\frac{4a^3}{3c_0^3} + \frac{2}{3}\sum_i \lambda_{\mathrm{r}i}^{-3}\right), \tag{4.4}$$

where the coefficients $\lambda_{\mathrm{r}i}$ have a positive real-valued part. It is noted that it is enough to consider one coefficient λ_{r} or a complex conjugated pair [9]. Assuming a constant reflection factor $2\ln\frac{1}{|\Gamma|} = \pi K$, over the bandwidth $1 - B/2 \le \omega/\omega_0 \le 1 + B/2$ gives

$$K\frac{B}{1 - B^2/4} = 2k_0a - 2\frac{\omega_0}{\lambda_{\mathrm{r}}} \tag{4.5}$$

and

$$K\frac{B + B^3/12}{(1 - B^2/4)^3} = \frac{4(k_0a)^3}{3} + \frac{2}{3}\frac{\omega_0^3}{\lambda_{\mathrm{r}}^3} \tag{4.6}$$

where $k_0 = \omega_0/c_0$. These equations are solved with respect to B and λ_{r}, in Figure 4, the solution B is depicted for a SWR of 2, *i.e.*, $|\Gamma| = 1/3$. For the narrow bandwidth case $B \ll 1$ the equalities can be combined as

$$\begin{aligned} KB \le{}& \frac{4(k_0a)^3}{3} + \frac{2}{24}(2k_0a - KB)^3 = \\ & \frac{4(k_0a)^3}{3} + \frac{2}{24}\big(8(k_0a)^3 - 12(k_0a)^2KB + 6k_0a(KB)^2 - (KB)^3\big) \le 2(k_0a)^3. \end{aligned} \tag{4.7}$$

This gives the asymptotic bandwidth

$$B \le \frac{\pi}{\ln|\Gamma|^{-1}}(k_0a)^3 \quad \text{for } B \ll 1, \tag{4.8}$$

see also Figure 4.

In theory, the equivalent circuits can be used to derive a Fano bandwidth for any TM_{mn} or TE_{mn} mode. However, this is rather tedious due to the complex structure of these higher order modes together with the non-linearity of the Fano theory.

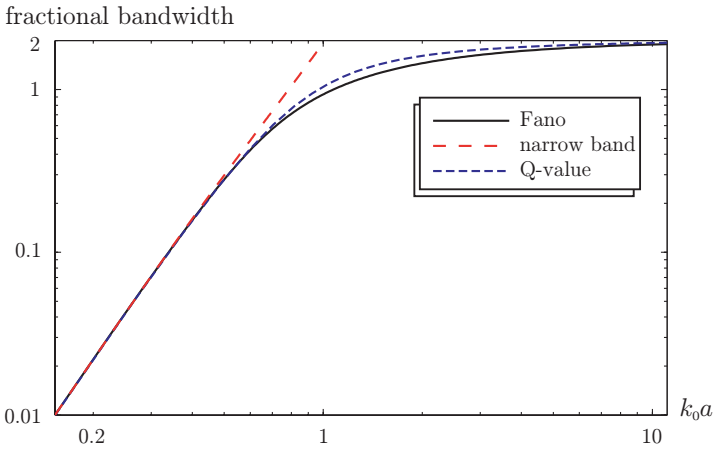

Figure 4: Fano fractional bandwidth as function of the sphere radius k_0a for a SWR of 2.

Moreover, it is known that it is advantageous to mix the TE and TM modes in high bandwidth systems [14]. Instead of using the analytic expression of the impedance it is common to use the Q-factor (quality factor, antenna Q or radiation Q) to get an estimate of the bandwidth. Since, there is an extensive literature on the Q-factor for antennas, see *e.g.*, [5, 6, 10, 12–14, 18], only some of the results are given here. The Q of the antenna is defined as the quotient between the power stored in the reactive field and the radiated power [5, 14]

$$Q = \frac{2\omega \max(W_{\mathrm{M}}, W_{\mathrm{E}})}{P}, \tag{4.9}$$

where ω is the angular frequency, W_{M} stored magnetic energy, W_{E} stored electric energy, and P the dissipated power. At the resonance frequency, there are equal amounts of stored electric energy and stored magnetic energy, *i.e.*, $W_{\mathrm{E}} = W_{\mathrm{M}}$. The Q-factor is related to the bandwidth of the corresponding resonance circuit as $\Delta f/f_0 \approx Q^{-1}$ for $Q \gg 1$. The Q-factor can either be determined by the equivalent circuits [5, 14] or by an analytic expression functions [6]. The Q of the TM_{lm} or TE_{lm} mode is given by

$$Q_l = ka - \left(\frac{(ka)^3}{2} + (l+1)ka\right)\left(\mathrm{j}_l^2 + \mathrm{y}_l^2\right) - \frac{(ka)^3}{2}\left(\mathrm{j}_{l+1}^2 + \mathrm{y}_{l+1}^2\right) + \frac{2l+3}{2}(ka)^2\left(\mathrm{j}_l\mathrm{j}_{l+1} + \mathrm{y}_l\mathrm{y}_{l+1}\right), \tag{4.10}$$

where j_l and y_l are the spherical Bessel and Neumann functions, respectively [6]. The Q-factor depends only on the l-index and there are $2(2l+1)$ modes for each l index, see Figure 5a. The six lowest order modes have $Q = (ka)^{-3} + (ka)^{-1}$. By combination of one TE_{m1} mode and one TM_{m1} mode the Q-factor is reduced to $Q = (ka)^{-3}/2 + (ka)^{-1}$.

At and around the resonance frequency, $\omega_0 = 2\pi f_0$, the antenna model is given by a resonance circuit, see Figure 3. The impedance of the antenna is only matched

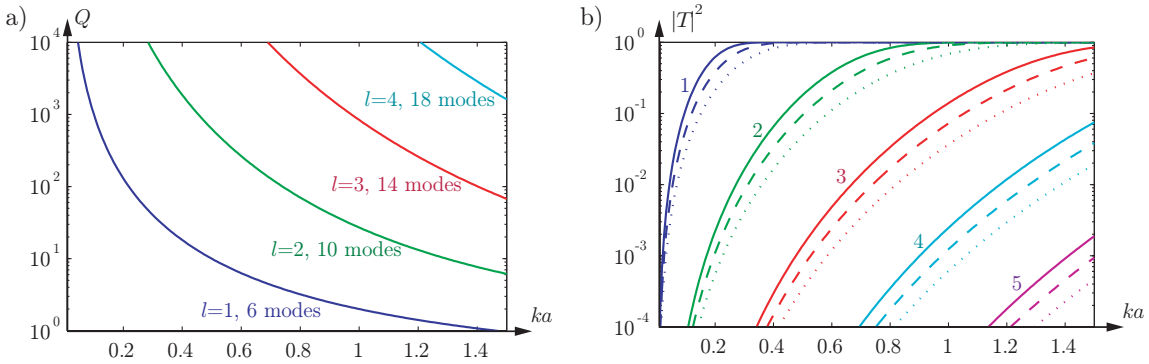

Figure 5: a) Q-factor as a function of the sphere radius ka. b) transmission coefficient $|T|^2$ in (4.19) as a function of ka for bandwidths of 5%, 10%, and 20%.

to the feeding network at the resonance frequency. For frequencies around the resonance frequency, the radiated power is given by $P_{\text{rad}} = |T|^2 P_{\text{in}} = (1 - |\Gamma|^2) P_{\text{in}}$. The transmission coefficient of the RCL circuits in Figure 3, is

$$t_{\text{RCL}}(s) = \frac{1}{1 + \frac{Q}{2}\left(\frac{\omega_0}{s} + \frac{s}{\omega_0}\right)}. \tag{4.11}$$

It has a single zero at the origin and a single zero at infinity. The corresponding reflection coefficient is

$$\Gamma_{\text{RCL}}(s) = \frac{1 + (s/\omega_0)^2}{1 + (s/\omega_0)^2 + \frac{2s}{\omega_0 Q}} \tag{4.12}$$

with the zeros and poles

$$\lambda_{\text{o}1,2} = \pm \text{i}\omega_0 \quad \text{and } \lambda_{\text{p}1,2} = \frac{\omega_0}{Q}\left(-1 \pm \text{i}\sqrt{Q^2 - 1}\right), \tag{4.13}$$

respectively. The Fano theory gives the integral relations

$$\frac{2}{\pi}\int_0^\infty \frac{1}{\omega^2} \ln \frac{1}{|\Gamma(\text{i}\omega)|}\, \text{d}\omega = \sum_i \lambda_{\text{o}i}^{-1} - \lambda_{\text{p}i}^{-1} - 2\lambda_{\text{r}i}^{-1} = \frac{2}{\omega_0 Q} - 2\sum_i \lambda_{\text{r}i}^{-1} \tag{4.14}$$

and

$$\frac{2}{\pi}\int_0^\infty \ln \frac{1}{|\Gamma(\text{i}\omega)|}\, \text{d}\omega = \sum_i \lambda_{\text{o}i} - \lambda_{\text{p}i} - 2\lambda_{\text{r}i} = 2\frac{\omega_0}{Q} - 2\sum_i \lambda_{\text{r}i} \tag{4.15}$$

by Taylor expansions around $s = 0$ and $s = \infty$, respectively. Assume that the matched reflection coefficient is constant over its bandwidth, *i.e.*, $\frac{2}{\pi}\ln\frac{1}{|\Gamma|} = K$, to get

$$\frac{B}{1 - B^2/4} K = \frac{2}{Q} - 2\sum_i \frac{\omega_0}{\lambda_{\text{r}i}} \quad \text{and } BK = \frac{2}{Q} - 2\sum_i \frac{\lambda_{\text{r}i}}{\omega_0}, \tag{4.16}$$

where the coefficients $\lambda_{\text{r}i}$ have a positive real-valued part. By considering one complex conjugated pair, $\lambda_{\text{r}1} = \lambda_{\text{r}2}^*$ it is seen that the first relation gives an inequality which yields the least upper bound for K as

$$K \le \frac{2}{BQ}\left(1 - \frac{B^2}{4}\right). \tag{4.17}$$

Hence, the reflection coefficient and fractional bandwidth are bounded as

$$|\Gamma| \geq \mathrm{e}^{-\frac{\pi}{QB}(1-B^2/4)} \quad \text{and } B \leq \sqrt{Q^2K^2+4} - QK \approx \frac{\pi}{Q \ln |\Gamma|^{-1}}, \tag{4.18}$$

respectively. The corresponding transmission coefficient is bounded as

$$|T|^2 = 1 - |\Gamma|^2 \leq 1 - \mathrm{e}^{-\frac{2\pi}{QB}(1-B^2/4)}, \tag{4.19}$$

see also Figure 5b. In Figure 4, the Fano fractional bandwidth for the TM_{m1} and TE_{m1} modes with a SWR of 2 are compared with the narrow-band approximation $B \ll 1$ and the Q-factor approximation. In the figure, it is seen that both approximations are good for small $k_0 a$. The Q-factor over estimates the bandwidth for large $k_0 a$.

5 Capacity of a sphere in a Rayleigh channel

In this Section, we analyze how the fundamental limitations derived in Section 4 affect the capacity of a sphere. We use the signal model (3.12) over a fixed bandwidth Δf. The ergodic capacity, in b/s, is given by

$$\overline{C}_{\Delta f} = \mathcal{E}\left\{ \max_{\mathbf{R}_{ss}} \int_{f_1}^{f_2} \log_2 \det \left(\mathbf{I} + \frac{P_{\mathrm{tot}}}{N_0 N_{\mathrm{s}} \Delta f} \mathbf{\Sigma} \mathbf{H}_{\mathrm{w}} \mathbf{R}_{ss} \mathbf{H}_{\mathrm{w}}^{\mathrm{H}} \mathbf{\Sigma}^{\mathrm{H}} \right) \mathrm{d}f \right\}, \tag{5.1}$$

where $P_{\mathrm{tot}}/(N_{\mathrm{s}}\Delta f)$ is the average power per plane wave and Hz. The matrix $\mathbf{R}_{ss}$ is given by the space–frequency water-filling solution (A.10). The communication scheme can, *e.g.*, be the OFDM, see Appendix A and [3, 4, 23]. To simplify the analysis, we consider the capacity efficiency over a bandwidth B, *i.e.*,

$$\overline{C}_{\mathrm{B}} = \mathcal{E}\left\{ \max_{\mathbf{R}_{ss}} \log_2 \det \left(\mathbf{I} + \frac{P}{N_0 N_{\mathrm{s}}} \mathbf{\Sigma} \mathbf{H}_{\mathrm{w}} \mathbf{R}_{ss} \mathbf{H}_{\mathrm{w}}^{\mathrm{H}} \mathbf{\Sigma}^{\mathrm{H}} \right) \right\}, \tag{5.2}$$

where $P = P_{\mathrm{tot}}/\Delta f$ is the power density. The matrix $\mathbf{R}_{ss}$ is given by the water-filling solution [21, 27]a and, hence, $\overline{C}_{\Delta f} \geq \overline{C}_B \Delta f = \overline{C}_B B f_0$.

In contrary to the fixed frequency case (3.15) where the singular values could be chosen to unity in the uncorrelated case, the singular values in (5.1) are limited by the required bandwidth. The Fano limit (4.18) on the reflection factor shows that the singular values are bounded by

$$\sigma_m^2 = 1 - |\Gamma_m|^2 = 1 - \mathrm{e}^{-\frac{2\pi}{Q_m B}(1-B^2/4)}, \tag{5.3}$$

where Q_m is the Q-factor of port number m. Here, one observes that the singular values σ_m^2 are small if the product between the Q-factor and the fractional bandwidth is large. The classical bandwidth definition of VSWR = 2 corresponds to a singular value $\sigma_m^2 = 8/9$.

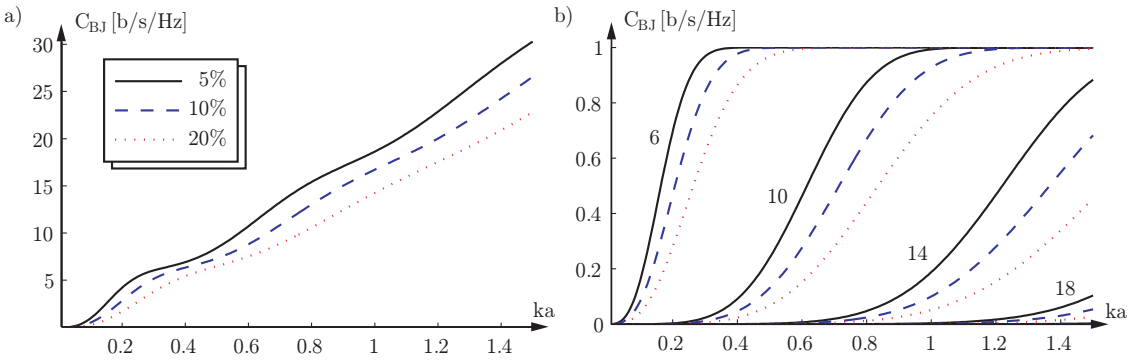

Figure 6: Capacity efficiency C_{BJ} of an idealized mode coupled antenna as a function of the radius ka for the bandwidths 5%, 10%, and 20% estimated with (5.5). a) the capacity efficiency. b) the capacity efficency of each mode.

We consider the case with no channel knowledge, $\mathbf{R}_{ss} = \mathbf{I}$. The Jensen inequality can be used to estimate the capacity [29], *i.e.*,

$$\overline{C}_{\mathrm{B}} \leq C_{\mathrm{BJ}} = \log_2 \det \left(\mathbf{I} + \frac{P \boldsymbol{\Sigma} \mathcal{E} \left\{ \mathbf{H}_{\mathrm{w}} \mathbf{H}_{\mathrm{w}}^{\mathrm{H}} \right\} \boldsymbol{\Sigma}^{\mathrm{H}}}{N_0 N_{\mathrm{s}}} \right) = \sum_{m=1}^{N_{\mathrm{y}}} \log_2 \left(1 + \frac{P}{N_0} \sigma_m^2 \right). \quad (5.4)$$

The upper bound C_{BJ}, in b/s/Hz, is deterministic and depends only on the properties of the receiving antenna channel and the SNR. For the case of a large number of uncorrelated incident waves, *i.e.*, N_{s} large, the inequality (5.4) becomes an equality since $\mathbf{H}_{\mathrm{w}} \mathbf{R}_{ss} \mathbf{H}_{\mathrm{w}}^{\mathrm{H}} = \mathbf{H}_{\mathrm{w}} \mathbf{H}_{\mathrm{w}}^{\mathrm{H}} \rightarrow N_{\mathrm{s}} \mathbf{I}_{N_{\mathrm{y}} \times N_{\mathrm{y}}}$ as $N_{\mathrm{s}} \rightarrow \infty$. Observe that estimate (5.4) is not good for $N_{\mathrm{y}} > N_{\mathrm{s}}$, it overestimates by the capacity by giving same results as for $N_{\mathrm{y}} \ll N_{\mathrm{s}}$. With the Fano estimate, (5.3), of the singular values, we get

$$C_{\mathrm{BJ}} = \sum_{m=1}^{N_{\mathrm{y}}} \log_2 \left(1 + \frac{P}{N_0} \left(1 - \mathrm{e}^{-\frac{2\pi}{Q_m B} \left(1 - \frac{B^2}{4} \right)} \right) \right) \quad (5.5)$$

as an expression of the capacity efficiency over a bandwidth B. Here, we observe that the capacity is limited by the product $Q_n B$.

For the idealized antenna connecting one spherical vector mode to one port, the explicit representation of the Q-factors can be used to calculate (5.5). The capacity C_{BJ} as a function of the sphere radius is depicted in Figure 6a for the bandwidths 5%, 10%, and 20%, an SNR of $P/N_0 = 1$, and an infinite number of antenna ports $N_{\mathrm{y}} = \infty$. As see in the figure, the capacity efficiency decreases with increased bandwidth. The capacity, in b/s, increases due to the multiplication with the bandwidth. It is also seen that the capacity increases rapidly with the size of the sphere. This is due the increased spatial diversity of the idealized antenna as seen in Figure 6b, where the capacity efficiency of each subchannel is shown. Only the first 6 modes, corresponding to $l = 1$, are used for a small sphere. For these modes it is also known that it is advantageous to combine the TE_{m1} and TM_{m1} modes since this doubles the radiation resistance and hence gives approximately half the Q-factor. For a larger sphere higher order modes can be used.

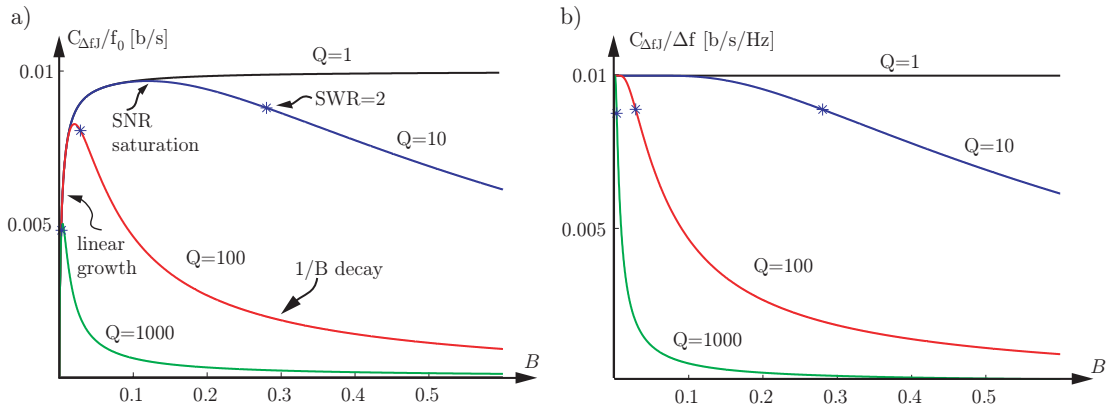

Figure 7: The capacity $C_{\Delta \mathrm{fJ}}$ as a function of the bandwidth for different Q-factors. The bandwidths related to $|\Gamma| = 1/3$ are indicated by the stars. a) the capacity in b/s with fixed total power $P_{\mathrm{tot}}/(N_0 f_0) = 0.01$. b) the capacity efficiency (in b/s/Hz) with fixed power density $P/N_0 = 0.01$.

It is also interesting to consider how the capacity, in b/s, for a fixed volume depends on the bandwidth. In this case it is natural to consider the total power $P_{\mathrm{tot}} = P\Delta f$ as fixed, this gives

$$C_{\Delta \mathrm{fJ}} = B f_0 \sum_{m=1}^{N_{\mathrm{y}}} \log_2 \left(1 + \frac{P_{\mathrm{tot}}}{N_0 f_0 B} \left(1 - \mathrm{e}^{-\frac{2\pi}{Q_m B}\left(1-\frac{B^2}{4}\right)} \right) \right). \tag{5.6}$$

The capacity (b/s) divided by the center frequency in (5.6) is plotted in Figure 7 for the scaled signal to noise ratio $P_{\mathrm{tot}}/(N_0 f_0) = 0.01$. Three regions can by identified in the figure. For sufficiently small fractional bandwidths BN_{y}, the capacity increases approximately linearly with BN_{y}. This is the region where MIMO systems have a large advantage, *i.e.*, the capacity increases almost linearly with the number of spatial channels N_{y}. For larger bandwidths the power in each channel gets small and the capacity is limited by the SNR.

5.1 MIMO cube and MIMO tetrahedron

To illustrate the antenna channel some simple idealized MIMO antennas are considered. The tripole antenna is probably the simplest MIMO antenna. It consists of three orthogonal electric dipoles and three orthogonal magnetic dipoles [2, 7], *i.e.*, the first six modes, $l = 1$, $m = -1, 0, 1$, and $\tau = 1, 2$. To avoid the problem of feeding both electric and magnetic dipoles, a MIMO cube [1] or a MIMO tetrahedron can be used, see Figure 8.

The MIMO tetrahedron consists of six electric dipoles centered on the edges of a tetrahedron. This gives a maximum of six ports for the antenna, *i.e.*, $N_{\mathrm{x}} = 6$ in transmission mode and $N_{\mathrm{y}} = 6$ in receive mode. The transmitting antenna channel $\mathbf{H}_{\mathrm{T}}$ can be determined by a projection of the far-field patterns of each dipole on the spherical vector modes. The transmitter is assumed be matched at the considered

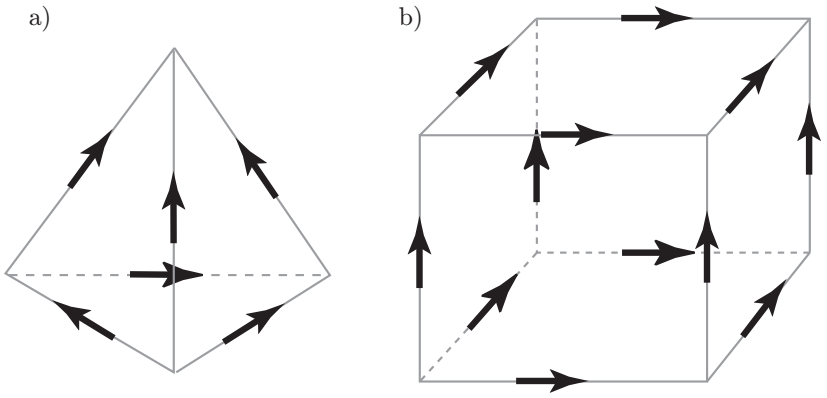

Figure 8: Illustration of MIMO antennas. a) a MIMO tetrahedron, *i.e.*, a tetrahedron with an electrical dipole on each edge. b) a MIMO cube, *i.e.*, a cube with an electrical dipole on each edge.

frequency and to conserve power. This gives a total channel gain $\|\mathbf{H}_{\mathrm{T}}\|_{\mathrm{F}}^2 = 6$. For a mismatched transmitter, the total channel gain is less than 6. Reciprocity gives the corresponding receiving channel as $\mathbf{H}_{\mathrm{R}} = \mathbf{H}_{\mathrm{T}}^{\mathrm{H}}$, where $\mathbf{H}_{\mathrm{R}}$ is a semi-infinite matrix with 6 rows. In Figure 9a, the mode representation of the MIMO tetrahedron with a side length of 0.3 wavelengths is depicted, *i.e.*, the rows of $\mathbf{H}_{\mathrm{R}}$. The amplitude of bar number α correspond to the magnitude of mode number α, where the modes are numbered as $\alpha = 2(l^2 + l - 1 + m) + \tau$, *i.e.*,

$$\begin{pmatrix} \alpha \\ l \\ m \\ \tau \end{pmatrix} = \begin{pmatrix} 1 & 2 & 3 & 4 & 5 & 6 & 7 & 8 & ... \\ 1 & 1 & 1 & 1 & 1 & 1 & 2 & 2 & ... \\ -1 & -1 & 0 & 0 & 1 & 1 & -2 & -2 & ... \\ 1 & 2 & 1 & 2 & 1 & 2 & 1 & 2 & ... \end{pmatrix} \tag{5.7}$$

As seen by the mode representation, both electric dipoles ($\tau = 2$) and magnetic dipoles ($\tau = 1$) are included in the representation. It is also observed that each dipoles excites several modes and that the amplitude decreases for large values of the l index.

The singular value decomposition is used to rewrite the radiation channel into a sum of orthogonal channels $\mathbf{H}_{\mathrm{R}} = \mathbf{U}\mathbf{\Sigma}\mathbf{V}^{\mathrm{H}}$. The mode excitations of the subchannels are given by the orthogonal semi-infinit matrix $\mathbf{V}$ of the SVD. In Figure 9b, the orthogonal channel, *i.e.*, the $\mathbf{\Sigma}\mathbf{V}^{\mathrm{H}}$, is depicted. Here, it is observed that the first three singular values $\sigma_{1,2,3}$ correspond to three orthogonal dipoles plus a small contribution from higher order modes. The next three singular values $\sigma_{4,5,6}$ correspond to the three orthogonal magnetic dipoles plus a small contribution from higher order modes.

In Figure 10a, the magnitude, $\log_2 \sigma_i^2$, of the singular values are potted as a function of the size of the tetrahedron. The $\log_2$ scale is used for a direct comparison with the loss in ergodic capacity. Here, it is seen that the electric dipoles dominate the radiation field if the tetrahedron is small, *e.g.*, the side less than 0.2 wavelengths. As the size of the tetrahedron increases the influence of the magnetic dipoles also increases. For a side length of 0.5 wavelengths the contribution from the electric

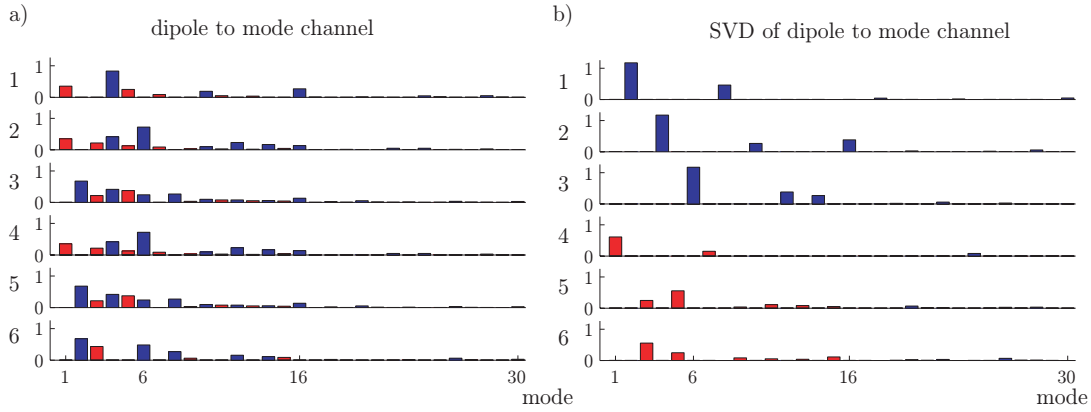

Figure 9: Mode representation of the MIMO tetrahedron with size 0.3λ for the first 30 modes, where (5.7) is used to order the modes. a) The mode representation for each dipole, *i.e.*, each graph represents one column of $\mathbf{H}_{\mathrm{T}}$ and the mode numbers represent the rows of $\mathbf{H}_{\mathrm{R}}$. b) The mode representation of the orthogonal channels *i.e.*, the rows and columns of $\mathbf{\Sigma V}^{\mathrm{H}}$. The first three and last three channels are dominated by electrical dipoles (odd modes) and magnetic dipoles (even modes), respectively.

dipoles and the magnetic dipoles are of the same magnitude. Observe, that there are only two different singular values, *i.e.*, $\sigma_1 = \sigma_2 = \sigma_3$ and $\sigma_4 = \sigma_5 = \sigma_6$.

To determine the capacity of the MIMO tetrahedron in a Rayleigh channel (3.12) is used. In Figure 10b, the ergodic capacity for the SNR values of $100, 10, 1, 0.1$, and 0.01 (simulated over 1000 realizations) is compared between the MIMO tetrahedron (solid lines), high SNR approximation (dashed lines), and the uncorrelated cases (dotted lines). In the figure, it is seen that the high SNR approximation is accurate for large antennas and a SNR above 1. The corresponding average number of used channels is shown in Figure 10c.

The MIMO cube consists of 12 electric dipoles centered on the edges of a cube. In [1], it is shown that the MIMO cube has 12 independent channels if the cube is sufficiently large. This is also observed in Figure 10d where gain of each channel is plotted as a function of the radius of the smallest sphere containing the dipoles. In the figure, it is seen that a small cube is dominated by first three channels. The ergodic capacity and the number of used channels as a function of the sphere radius are shown in Figure 10 e and f, respectively.

6 Conclusions

The analysis of the spectral efficiency in this paper reveals that it is important to consider a model that incorporates the properties of the antennas and the matching network. As shown in (3.15), the ergodic capacity at a fixed frequency, *i.e.*, capacity in b/s/Hz, is independent of the size of the sphere. This means that, at least in theory, it would be possible to design small antenna with high spatial diversity. The drawback of small antennas such as being narrow band and lossy are well known [13,

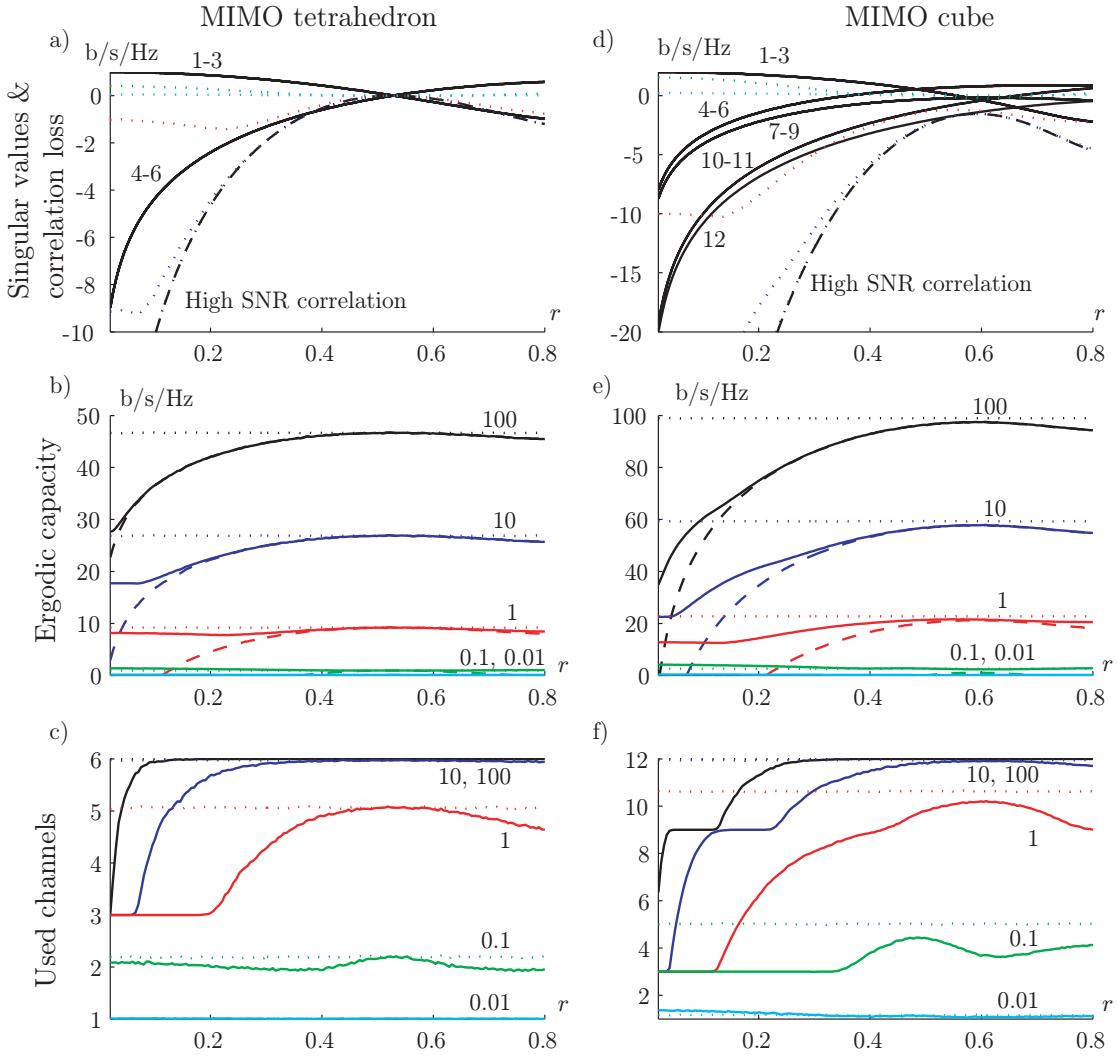

Figure 10: Properties of the MIMO tetrahedron (a to c) and the MIMO cube (d to f) as a function of the antenna radius for SNR values of $100, 10, 1, 0.1$, and 0.01. a) the singular value distribution where each solid line corresponds to three singular values. The dashed and dotted lines show the correlation loss of ergodic capacity in a high SNR case (3.16) and the SNR values above, respectively. b) Comparison between the ergodic capacity of the MIMO tetrahedron (solid lines), high SNR approximation (dashed lines), and uncorrelated case (dotted lines). c) Comparison of the average number of used channels of the MIMO tetrahedron case and the non-correlated case. d) to f) the corresponding cases for the MIMO cube.

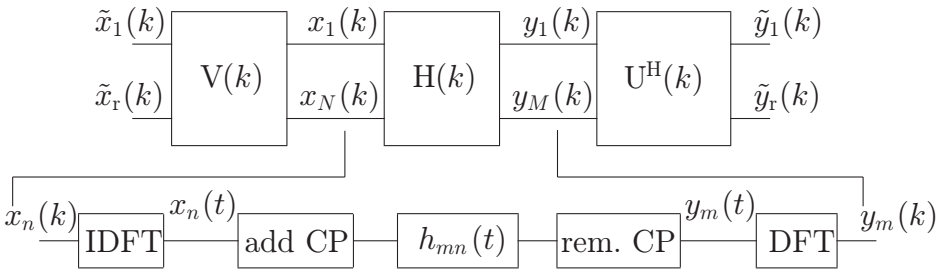

Figure 11: The baseband MIMO–OFDM system.

27]. These drawbacks are naturally included in the analysis by consideration of the capacity over a bandwidth, *i.e.*, capacity in b/s.

The analysis is based on several assumptions. The Rayleigh type channel is widely used in the literature and it is also used here due to its simple closed form solutions. However, it is probably to simple for a realistic MIMO channel model. The use of spherical vector modes to model an arbitrary antenna is standard in antenna theory. Here, we assume that each mode or a simple linear combination of modes are connected to one port by a lossless matching network. This lets us use the Fano theory to relate the bandwidth to the reflection coefficient of the system. It is well known that resistive loading of the antenna can be used to trade efficiency for bandwidth. Hence, it would be desired to use a Fano-type theory for lossy matching networks. Moreover, it would be interesting to include an arbitrary multi-port matching network.

Acknowledgments

The financial support by the Swedish research council is gratefully acknowledged. The authors would like to express their gratitude to Prof. George Papanicolaou for the opportunity to visit his group at the Mathematics Department, Standford University, during Mars 2003, and the many fruitful discussions on wave propagation and statistical signal processing from which the present paper has emanated.

Appendix A Channel capacity and MIMO–OFDM communication

The MIMO signal model in (2.1) can represent many communication schemes, see *e.g.*, [11, 23]. However, in our view, the most fundamental as well as the most technically straightforward is the MIMO–OFDM communication scheme which is briefly outlined below, see also [3, 4, 23]. We use the OFDM framework together with a limiting argument to derive an expression for the optimum channel capacity, and we emphasize that the OFDM strategy is a practical means of approximating this optimum capacity. We will later use the general expression for channel capacity to derive upper bounds for the capacity of a channel decomposition.

The baseband, discrete–time MIMO–OFDM system consisting of N transmitting and M receiving antennas is depicted in Figure 11. Here $x_n(t)$ and $y_m(t)$ denote the transmitted and received antenna signals, respectively, and $h_{mn}(t)$ denotes the impulse response connecting the transmitting antenna n to the receiving antenna m. The bandwidth of the channel is Δf, the symbol time for each channel use is $T = \frac{1}{\Delta f}$ and the symbol rate $f_s = 1/T$ is thus equal to the *Nyquist rate* Δf.

Let the total delay spread of the multi–path channel be denoted τ_d. Given that the cyclic prefix $CP > \tau_d f_s$, linear convolution becomes identical with circular convolution over the entire DFT–frame [3], and we have

$$y_m(t) = \sum_{n=1}^{N_{\rm x}} h_{mn}(t) \otimes x_n(t) + n_m(t), \tag{A.1}$$

for $t \in [0, \frac{N_{\rm DFT}-1}{f_s}]$ where $N_{\rm DFT}$ is the size of the DFT and $m = 1, \ldots, N_{\rm y}$. Here $n_m(t)$ is assumed to be samples of complex Gaussian noise [20] with constant spectral density N_0 [W/Hz] over the entire bandwidth $[-W, W]$. The sampled noise $n_m(t)$ is uncorrelated due to the Nyquist–sampling, and the variance is $\sigma_v^2 = BN_0$. The sensor noise $n_m(t)$ is also assumed to be uncorrelated over the different sensors m. We assume that the discrete–time channel impulse response is scaled such that $h_{mn}(t) = Th^c_{mn}(t)$ so that $h_{mn}(k) = h^c_{mn}(\frac{k}{N_{\rm DFT}} f_s)$ where $h_{mn}(k)$ is the DFT of $h_{mn}(t)$, and $h^c_{mn}(t)$ is the corresponding continuous–time channel impulse response with frequency function $h^c_{mn}(f)$.

Taking the DFT of (A.1), we obtain

$$y_m(k) = \sum_{n=1}^{N_{\rm x}} h_{mn}(k)x_n(k) + v_m(k), \tag{A.2}$$

for $k \in [0, N_{\rm DFT} - 1]$, which can be written in matrix form as

$$\boldsymbol{y}(k) = \mathbf{H}(k)\boldsymbol{x}(k) + \boldsymbol{v}(k), \tag{A.3}$$

where $\boldsymbol{y}(k)$ is $N_{\rm y} \times 1$, $\boldsymbol{x}(k)$ is $N_{\rm x} \times 1$, $\boldsymbol{v}(k)$ is $N_{\rm y} \times 1$, and $\mathbf{H}(k)$ is $N_{\rm y} \times N_{\rm x}$.

Next, we assume that the DFT's $\boldsymbol{y}(k)$, $\boldsymbol{x}(k)$, and $\boldsymbol{v}(k)$ are scaled with the factor $\frac{1}{\sqrt{N_{DFT}}}$ so that time averages become equal to frequency averages. Hence, $\mathcal{E}\left\{|v_m(t)|^2\right\} = \mathcal{E}\left\{|v_m(k)|^2\right\} = \sigma_v^2 = BN_0$. The correlation matrix of the noise vector $\boldsymbol{v}(k)$ is thus given by $\mathcal{E}\left\{\boldsymbol{v}(k)\boldsymbol{v}^H(k)\right\} = \sigma_v^2\mathbf{I}$. Note that since the noise $v_m(t)$ is Gaussian and uncorrelated over time, the noise $v_m(k)$ is also Gaussian and uncorrelated over frequency. Hence, (A.2) represents $N_{\rm DFT}$ independent communication channels. The DFT has accomplished an orthogonalization over frequency.

The orthogonalization over space is accomplished by the singular value decomposition (SVD) of the channel matrix $\mathbf{H}(k)$

$$\mathbf{H}(k) = \mathbf{U}(k)\mathbf{\Sigma}(k)\mathbf{V}^H(k) \tag{A.4}$$

where $\mathbf{U}(k)$ and $\mathbf{V}(k)$ contain the left and right singular vectors, respectively, $\mathbf{\Sigma}(k)$ contain the singular values $\sigma_i(k)$ for $i = 1, \ldots, r(k)$ and $r(k)$ is the rank of the channel. By defining $\tilde{\boldsymbol{y}}(k) = \mathbf{U}^H(k)\boldsymbol{y}(k)$, $\tilde{\boldsymbol{x}}(k) = \mathbf{V}^H(k)\boldsymbol{x}(k)$, and $\tilde{\boldsymbol{v}}(k) = \mathbf{U}^H(k)\boldsymbol{v}(k)$ we

obtain the diagonalized system

$$\tilde{\boldsymbol{y}}(k) = \boldsymbol{\Sigma}(k)\tilde{\boldsymbol{x}}(k) + \tilde{\boldsymbol{v}}(k) \tag{A.5}$$

where the correlation matrix of $\tilde{\boldsymbol{v}}(k)$ is $\mathcal{E}\left\{\tilde{\mathbf{v}}(k)\tilde{\boldsymbol{v}}^H(k)\right\} = \mathcal{E}\left\{\boldsymbol{v}(k)\mathbf{v}^H(k)\right\} = \sigma_v^2\mathbf{I}$. Hence, the noise term $\tilde{v}_m(k)$ is complex Gaussian and uncorrelated over both frequency and space. The system in (A.5) therefore represents $r(k)$ independent communication channels for each frequency bin k.

Neglecting the cyclic prefix for a moment, and considering the OFDM frames consisting of N_{DFT} samples during $N_{\mathrm{DFT}}T$ seconds, the total channel capacity for the system in (A.5) is given by

$$C_{\mathrm{tot}} = \frac{1}{N_{\mathrm{DFT}}T} \sum_{k=0}^{N_{\mathrm{DFT}}-1} \sum_{i=1}^{r(k)} \log_2\left(1 + P_i(k)\frac{\sigma_i^2(k)}{BN_0}\right) \quad [\text{bits/sec}] \tag{A.6}$$

where $P_i(k) = E\{|\tilde{x}_i(k)|^2\}$ is chosen as the optimum space–frequency water-filling solution

$$P_i(k) = \left(\xi - \frac{BN_0}{\sigma_i^2(k)}\right)^+ \tag{A.7}$$

and ξ is chosen to satisfy the maximum power constraint

$$\frac{1}{N_{\mathrm{DFT}}} \sum_{k=0}^{N_{\mathrm{DFT}}-1} \sum_{i=1}^{r(k)} P_i(k) = P. \tag{A.8}$$

The total power P is in [W] and the quantity $\frac{P_i(k)}{N_{\mathrm{DFT}}}$ is in [W/bin].

By letting the cyclic prefix be of fixed length, and by taking the limit of (A.6), (A.7) and (A.8) as $N_{DFT} \to \infty$, we get the optimum channel capacity over a bandwidth of $B = 2W$. Hence, let $f_k = \frac{k}{N_{\mathrm{DFT}}}f_s \to f$, $\frac{1}{N_{\mathrm{DFT}}T} = \mathrm{d}f$, $r(k) \to r(f)$, $TP_i(k) \to P_i(f)$ and $\sigma_i(k) = \sigma_i(f_k) \to \sigma_i(f)$ where $\sigma_i(f)$ denotes the singular values of the continuous–time channel. The optimum channel capacity is then

$$C_{\mathrm{tot}} = \int_{-W}^{W} \sum_{i=1}^{r(f)} \log_2\left(1 + P_i(f)\frac{\sigma_i^2(f)}{N_0}\right) \mathrm{d}f \quad [\text{bits/sec}] \tag{A.9}$$

where $P_i(f)$ is chosen as the optimum space–frequency water-filling solution

$$P_i(f) = (\eta - \frac{N_0}{\sigma_i^2(f)})^+ \tag{A.10}$$

and η is chosen to satisfy the maximum power constraint

$$\int_{-W}^{W} \sum_{i=1}^{r(f)} P_i(f)\,\mathrm{d}f = P. \tag{A.11}$$

The total power P is in [W] and the quantity $P_i(f)$ is in [W/Hz]. For a random channel the information rate of the channel is random. The ergodic capacity of the

channel is the ensemble average over the channel, *i.e.*,

$$\overline{C}_{\text{tot}} = \mathcal{E}\left\{\int_{-W}^{W}\sum_{i=1}^{r(f)}\log_2\left(1+P_i(f)\frac{\sigma_i^2(f)}{N_0}\right)\mathrm{d}f\right\}. \tag{A.12}$$

Appendix B An inequality for the singular values of matrix products

Theorem B.1. Let $C(\mathbf{H}(f))$ denote the capacity of a frequency dependent channel as defined by (A.9) through (A.11) where $\sigma_i(f)$ denotes the singular values of the channel $\mathbf{H}(f)$. The capacity of the channel decomposition

$$\mathbf{H}(f) = \prod_{k=1}^{n}\mathbf{H}_k(f) \tag{B.1}$$

is then bounded by

$$C\left(\mathbf{H}(f)\right) \le \min_{k\in\{1,\ldots,n\}} C\left(\mathbf{H}_k(f)\prod_{j\neq k}\|\mathbf{H}_j(f)\|\right). \tag{B.2}$$

□

Proof: Let $\sigma_i(\mathbf{H}_k(f))$ denote the singular values of the subchannel $\mathbf{H}_k(f)$. Repeated use of the inequalities $\sigma_i(\boldsymbol{AB}) \le \sigma_i(\boldsymbol{A})\|\mathbf{B}\|$ and $\sigma_i(\boldsymbol{AB}) \le \sigma_i(\mathbf{B})\|\boldsymbol{A}\|$ for the product of matrices (see appendix A) yields the inequality

$$\sigma_i(\mathbf{H}_1(f)\cdots\mathbf{H}_k(f)\cdots\mathbf{H}_n(f)) \le \sigma_i(\mathbf{H}_k(f))\prod_{j\neq k}\|\mathbf{H}_j(f)\|. \tag{B.3}$$

or

$$\sigma_i(\mathbf{H}(f)) \le \sigma_i\left(\mathbf{H}_k(f)\prod_{j\neq k}\|\mathbf{H}_j(f)\|\right). \tag{B.4}$$

Let $P_i(f)$ denote the optimum power strategy to obtain the capacity on left side of (B.2). The inequality (B.2) then follows immediately from (B.4), the definition of capacity (A.9) through (A.11) and the monotonicity of the logarithm function.□

Theorem B.2. Let $\mathbf{A}$ and $\mathbf{B}$ be $m\times p$ and $p\times n$ matrices, respectively, and let $q = \min\{m,n,p\}$. Let r be the rank of the matrix $\mathbf{AB}$ where $r \le q$. Let $\sigma_i(\mathbf{A})$ denote the singular values of the matrix $\mathbf{A}$ in decreasing order, i.e. $\sigma_1(\mathbf{A}) \ge \sigma_2(\mathbf{A}) \ge \ldots \ge 0$, and let $\sigma_i(\mathbf{B})$ and $\sigma_i(\mathbf{AB})$ be similarly defined. Then the following inequality hold

$$\sigma_{i+j-1}(\mathbf{AB}) \le \sigma_i(\mathbf{A})\sigma_j(\mathbf{B}), \quad 1\le i,j\le r,\ i+j-1\le r \tag{B.5}$$

and in particular

$$\sigma_i(\mathbf{AB}) \le \sigma_i(\mathbf{A})\sigma_1(\mathbf{B}) = \sigma_i(\mathbf{A})\|\mathbf{B}\|, \quad 1\le i\le r \tag{B.6}$$

$$\sigma_j(\mathbf{AB}) \le \sigma_1(\mathbf{A})\sigma_j(\mathbf{B}) = \sigma_j(\mathbf{B})\|\mathbf{A}\|, \quad 1\le j\le r \tag{B.7}$$

where $\|\cdot\|$ denotes the matrix norm (maximum singular value). □

Proof: The proof of the theorem is given in [15] for the case where $m = n$ and $r \leq \min\{m, p\}$. Here, we show the more general result by employing the theorem in [15] in which $\mathbf{A}$ and $\mathbf{B}^T$ have the same dimension. By extending with zeros the rows and columns of a general $m \times p$ matrix $\mathbf{A}$ and by examining its singular value decomposition, it is readily verified that

$$\sigma_i(\begin{bmatrix} \mathbf{A} \\ \mathbf{0} \end{bmatrix}) = \sigma_i(\mathbf{A}), \quad 1 \leq i \leq r \tag{B.8}$$

$$\sigma_i(\begin{bmatrix} \mathbf{A} & \mathbf{0} \end{bmatrix}) = \sigma_i(\mathbf{A}), \quad 1 \leq i \leq r \tag{B.9}$$

where $\mathbf{0}$ is a zero matrix of suitable dimension and r is the rank of $\mathbf{A}$. Using this result, and the above mentioned theorem in [15], we can establish the following inequality for $m \geq n$

$$\sigma_{i+j-1}(\mathbf{AB}) = \sigma_{i+j-1}(\mathbf{A}\begin{bmatrix} \mathbf{B} & \mathbf{0} \end{bmatrix}) \leq \sigma_i(\mathbf{A})\sigma_j(\begin{bmatrix} \mathbf{B} & \mathbf{0} \end{bmatrix}) = \sigma_i(\mathbf{A})\sigma_j(\mathbf{B}) \tag{B.10}$$

where the zero matrix is chosen such that $\begin{bmatrix} \mathbf{B} & \mathbf{0} \end{bmatrix}$ is $p \times m$. The inequality is valid for $i \leq r$, $j \leq r$ and $i + j - 1 \leq r$ where r is the rank of $\mathbf{AB}$. This shows the validity of (B.5).

For $m \leq n$ we get

$$\sigma_{i+j-1}(\mathbf{AB}) = \sigma_{i+j-1}(\begin{bmatrix} \mathbf{A} \\ \mathbf{0} \end{bmatrix}\mathbf{B}) \leq \sigma_i(\begin{bmatrix} \mathbf{A} \\ \mathbf{0} \end{bmatrix})\sigma_j(\mathbf{B}) = \sigma_i(\mathbf{A})\sigma_j(\mathbf{B}) \tag{B.11}$$

where the zero matrix is chosen such that $\begin{bmatrix} \mathbf{A} \\ \mathbf{0} \end{bmatrix}$ is $n \times p$. The inequality is valid for $i \leq r$, $j \leq r$ and $i + j - 1 \leq r$ where r is the rank of $\mathbf{AB}$. Again, this shows the validity of (B.5). □

References

[1] J. B. Andersen and B. N. Getu. The MIMO cube - a compact MIMO antenna. In *Wireless Personal Multimedia Communications, 2002. The 5th International Symposium on*, volume 1, pages 112–114. IEEE, 2002.

[2] M. R. Andrews, P. P. Mitra, and R. de Carvalho. Tripling the capacity of wireless communications using electromagnetic polarization. *Nature*, **409**, 316–318, January 2001.

[3] J. A. C. Bingham. Multicarrier modulation for data transmission: An idea whose time has come. *IEEE Communications Magazine*, **28**, 5–14, May 1990.

[4] R. S. Blum, Y. G.Li, J. H. Winters, and Q. Yan. Improved space-time coding for mimo-ofdm wireless communications. *IEEE Transactions on Communications*, **49**(11), 1873–1878, November 2001.

[5] L. J. Chu. Physical limitations of Omni-Directional antennas. *Appl. Phys.*, **19**, 1163–1175, 1948.

[6] R. E. Collin and S. Rothschild. Evaluation of antenna Q. *IEEE Trans. Antennas Propagat.*, **12**, 23–27, January 1964.

[7] R. T. Compton. The tripole antenna: An adaptive array with full polarization flexibility. *IEEE Trans. Antennas Propagat.*, **29**(6), 944–952, November 1981.

[8] P. F. Driessen and G. J. Foschini. On the capacity formula for multiple input-multiple output wireless channels: A geometric interpretation. *IEEE Trans. on Communication*, **47**(2), 173–176, February 1999.

[9] R. M. Fano. Theoretical limitations on the broadband matching of arbitrary impedances. *Journal of the Franklin Institute*, **249**(1,2), 57–83 and 139–154, 1950.

[10] R. L. Fante. Quality factor of general antennas. *IEEE Trans. Antennas Propagat.*, **17**(2), 151–155, March 1969.

[11] G. J. Foschini and M. J. Gans. On limits of wireless communications in a fading environment when using multiple antennas. *Wireless Personal Communications*, **6**, 311–335, 1998.

[12] W. Geyi, P. Jarmuszewski, and Y. Qi. The Foster reactance theorem for antennas and radiation Q. *IEEE Trans. Antennas Propagat.*, **48**(3), 401–408, March 2000.

[13] R. C. Hansen. Fundamental limitations in antennas. *Proc. IEEE*, **69**(2), 170–182, 1981.

[14] R. F. Harrington. *Time Harmonic Electromagnetic Fields*. McGraw-Hill, New York, 1961.

[15] R. A. Horn and C. R. Johnson. *Topics in Matrix Analysis*. Cambridge University Press, 1991.

[16] W. C. Jakes and D. Cox. *Microwave Mobile Communications*. IEEE Press, 1994.

[17] S. Loyka. Information theory and electromagnetism: Are they related? In *COST 273/284 Workshop on Antennas and Related System Aspects in Wireless Communications*, Gothenburg, Sweden, June 2004.

[18] J. S. McLean. A re-examination of the fundamental limits on the radiation Q of electrically small antennas. *IEEE Trans. Antennas Propagat.*, **44**(5), 672–676, May 1996.

[19] D. A. B. Miller. Communicating with waves between volumes: evaluating orthogonal spatial channels and limits on coupling strengths. *Appl. Opt.*, **39**(11), 1681–1699, April 2000.

[20] K. S. Miller. *Complex Stochastic Processes*. Addison–Wesley Publishing Company, Inc., 1974.

[21] A. Paulraj, R. Nabar, and D. Gore. *Introduction to Space-Time Wireless Communications*. Cambridge University Press, Cambridge, U.K., 2003.

[22] J. G. Proakis. *Digital Communications*. McGraw-Hill, third edition, 1995.

[23] G. G. Raleigh and J. M. Cioffi. Spatio-temporal coding for wireless communication. *IEEE Transactions on Communications*, **46**(3), 357–366, March 1998.

[24] C. E. Shannon. A mathematical theory of communication. *Bell System Technical Journal*, **27**, 379–423 and 623–656, July and October 1948.

[25] T. Svantesson. Correlations and channel capacity of MIMO systems employing multimode antennas. *IEEE Trans. Vehicular Technol.*, **51**(6), 1304–1312, 2002.

[26] A. Vassiliadis and R. L. Tanner. Evaluating the impedance broadbanding potential of antennas. *IRE Trans. on Antennas and Propagation*, **6**(3), 226–231, July 1958.

[27] R. Vaughan and J. Bach Andersen. *Channels, Propagation and Antennas for Mobile Communications*. Institution of Electrical Engineers, 2003.

[28] J. W. Wallace and M. A. Jensen. Intrinsic capacity of the MIMO wireless channel. In *Vehicular Technology Conference, 56th*, volume 2, pages 701–705. IEEE, 2002.

[29] M. Wennström. *On MIMO systems and adaptive arrays for wireless communication*. PhD thesis, Uppsala University, Sweden, 2002.